This is a repository copy of *Computation of Methane/air Ignition Delay and Excitation Times, using Comprehensive and Reduced Chemical Mechanisms and their Relevance in Engine Autoignition*.

White Rose Research Online URL for this paper:
http://eprints.whiterose.ac.uk/118598/

Version: Accepted Version

Computation of Methane/air Ignition Delay and Excitation Times, using Comprehensive and Reduced Chemical Mechanisms and their Relevance in Engine Autoignition.

Luke Bates[a], Derek Bradley[a], Inna Gorbatenko[a,b,c], Alison S. Tomlin[b]

[a]School of Mechanical Engineering, University of Leeds, Leeds, LS2 9JT, United Kingdom

[b]School of Chemical and Process Engineering, University of Leeds, Leeds, LS2 9JT, United Kingdom

[c]EPSRC CDT in Fluid Dynamics, University of Leeds, Leeds, LS2 9JT, United Kingdom

Corresponding author: d.bradley@leeds.ac.uk

Abstract

Ignition delay time, τ_i, and excitation time, τ_e, for CH_4/air mixtures are mathematically modelled, using a comprehensive chemical kinetic scheme and a reduced global model. A principal objective is to obtain relevant data for this important engine fuel, to assess its propensity to knocking combustion in comparison with that of other fuels. Severe knock is associated with an intense heat release rate during the excitation time, τ_e, short enough for it to feed into, and strengthen, the pressure wave arising from the rate of change of the heat release rate at a hot spot. This assessment is quantified by loci of possible hot spot autoignitions, relative to the detonation peninsula on a ξ/ε diagram based on τ_i and τ_e. A second objective is to assess the accuracy and practical usage of the reduced global model. Appropriate selection of the controlling parameters for the seven equation global model gave predictions of τ_i close to those of both the complete kinetic scheme and experimental data in the literature. Much smaller time increments are required for the modelling of τ_e, but even with separately selected rate parameterisations for the prediction of τ_i, and τ_e values, the global model predictions of τ_e were only within an order of magnitude of those from the comprehensive kinetic scheme. However, computational times were about ten times faster with the global model, rendering it suitable for the computation of τ_i within 3D reactive transport simulations. Stoichiometric CH_4/air displayed very good antiknock properties in comparison with other fuels under turbocharged engine running conditions. Data on τ_i and τ_e from several sources are combined with a tentative hot spot structure, to assess the proximity of the deflagrative and autoignitive regimes, and the bounds of the transition regime.

Keywords: methane, ignition delay time, excitation time, knocking propensity, kinetic modelling, global reaction scheme.

1. Introduction.

A simplistic model of autoignition assumes that, following instantaneous compression of a flammable uniform mixture, heat release occurs instantaneously in a thermal explosion at the strong ignition limit after an autoignition delay time, τ_i. During this time, any heat loss or heat release is negligible. In practice, different rapid compression machines, RCMs, have a range of compression times during which some reaction occurs. There is some release and loss of heat during the delay time. For all of these effects some allowance can be made [1], enabling corrections to be made to plots of τ_i against reciprocal temperature. Experimentally, there is some support for a simplistic modelling approach, in which both heat release and heat loss can be relatively small, although difficult to measure, and to some extent they are in balance. However, the mixture can never be completely homogeneous, and hot spot ignition can be initiated, typically, by a temperature elevation of the order of 1 K. After τ_i has elapsed, computations show a subsequent very rapid heat release rate. This necessitates a very significant decrease in the computational time increments in the mathematical modelling. In a seminal paper Lutz et al. [2] were able to obtain the temporal profile of heat release rate and its duration, the excitation time, τ_e [3]. Sufficiently accurate computation of this time requires a comprehensive chemical kinetic scheme that combines the chemical species equations with the energy equation. Values are usually in the microsecond range and cannot be measured experimentally.

Both τ_i and τ_e are important factors controlling potentially damaging knock in engines. This is initiated at a hot spot and requires sufficiently small values of τ_i and reactivity gradient to generate an autoignitive propagation velocity that is greater than the deflagrative burning velocity, and approaches

2

the acoustic velocity [4]. If the mixture is insufficiently autoignitive, a deflagrative flame propagation may ensue, rather than a full autoignition. This aspect is discussed further in Section 5.3. The rate of change of the heat release rate at a hot spot generates a pressure pulse [5] and if τ_e is small enough to feed sufficient energy into the pressure pulse, the pulse can be amplified to generate a developing detonation.

Methane was studied because of its widespread distribution and usage in heating and power generation. The chemical kinetics of its oxidation are reasonably well understood, rendering predictions based on recently developed chemical mechanisms fairly reliable when compared to many larger hydrocarbon fuels. Here are compared predictions based on the widely used GRI Mech3.0 mechanism [6] with the more recently developed Mech_56.54 mechanism [7]. Accurate evaluations of τ_i and τ_e make it possible to assess the propensity of CH_4 to detonate.

The aims of the paper are:

(i) To study the autoignition and subsequent heat release of methane and the main contributing reactions, using detailed chemical kinetics.

(ii) Alongside this, to develop sufficiently accurate reduced global reaction schemes, for predicting τ_i and possibly τ_e, in order to conserve computational effort in large CFD applications.

(iii) To provide τ_e data for stoichiometric methane/air.

(iv) To discuss the remaining uncertainties in robustness of both detailed chemical mechanisms and reduced schemes, as well as the definition of τ_e.

(v) To demonstrate the practical value of such data, particularly, in the prediction of engine knock, detonation, and identification of the characteristics of the deflagrative, autoignitve, and transitional reaction regimes.

The present study of the autoignition of CH_4/air employs the Cantera Code, originally written and developed by Goodwin [8]. It is open source object orientated software that covers chemical kinetics, thermodynamics, and transport processes. It provides a framework for combustion modelling using detailed chemical reaction mechanisms, with numerous species, their various reaction pathways, and appropriate reaction rate constants. It is able to read and interpret a range of mechanisms and thermodynamic data formats, including those used by Chemkin [9] and NASA [10].

The computation of τ_i and τ_e with comprehensive chemical kinetic schemes is computationally demanding. In contrast, suitably tuned reduced global reaction schemes, employ much fewer species and reactions. This allows their use in applications such as reacting flow, where large comprehensive schemes are often prohibitively computationally expensive. The scheme employed in the present study

requires just five global reactions between six active species. With suitable tuning of the global rate constants, such schemes are capable of predicting ignition delay times over quite large ranges of temperature and pressure. The scheme is based on that of Schreiber et al. [11] and has a particular ability to predict τ_i for the Primary Reference Fuels, PRF, ioctane and nheptane. The schematic details are outlined in Table 1. The Octane number scaling factors of the original paper are omitted, allowing the model to be adapted for a fuller range of individual fuels. It is applicable to a broad range of fuels within its specified range of conditions. For non PRF, mixtures, the model must be matched to the fuels by further adjustment of the global rate constants.

The values of τ_i and τ_e, together with the computed activation temperatures, are employed in a comparison of the knocking propensity of different fuels, and also in a tentative attempt to define the transition regime lying between those of autoignitive and deflagrative propagations of reactions.

Table 1. Reduced Reaction Scheme. F: fuel, O_2: oxygen, P: product, Y: chain propagating species, X: chain branching species, I: product oxygenated radicals, molar ratio of O_2 to Fuel for desired equivalence ratio, a = 2 for CH_4.

Reaction Number	Reaction	Reaction Description
1 High Temperature	$F \rightarrow X$	Breakdown of fuel into branching intermediates
2 High Temperature	$X + aO_2 \rightarrow P$	Reaction of intermediates with oxygen to form products
3 Low Temperature	$F + 2O_2 \leftrightarrow I$	Reversible reaction converting between fuel and oxygen, and radical intermediate species
4 Low Temperature	$I \rightarrow 2Y$	Radicals react to form chain propagating intermediates
5 Low Temperature	$Y + 0.5F + (a-1)O_2 \rightarrow P$	Intermediates, fuel and oxygen react to form products.

In addition to the generation of new predictions of τ_i, τ_e and heat release rates, a primary purpose of the present paper is to compare the predictions of τ_i and τ_e, derived from both comprehensive chemical kinetic and reduced global schemes, such as might be employed in reactive flow models aiming to predict detonation behaviour. Stoichiometric CH_4/air mixtures are investigated between 0.1 and 10 MPa, and 700 and 1670 K. In the case of τ_i, comparisons are also made with experimental values from the literature. In the case of τ_e the accuracy of the determination of heat release rates is discussed. This enables the reliability and accuracy of the reduced global scheme to be assessed, as well as the antiknock characteristics of this important fuel, when compared with those of other fuels.

2. Computational Procedures

2.1 Comprehensive kinetic scheme

The Cantera software toolkit employed the Python programming language and the detailed chemical kinetic mechanism for CH_4/air reaction, Mech_56.54, of Burke et al. [7]. This is based on the AramcoMech1.3 mechanism [12]. Mech_56.54 [7] was developed in 2015, covering 113 species and 710 reactions. For convenience, for each set of conditions, the reactions are numbered consecutively in order of increasing endothermicity. The mechanism has been broadly validated against measurements in flow reactors, jet stirred reactors, and shock tubes for predictions of ignition delay times, burning velocities, and flame speciations for pressures, P, between 0.71 and 4.15 MPa over a range of temperatures, T, between 600 and 1600 K, at values of equivalence ratio, ϕ, from 0.3 to 2.0 [7].

For comparison, the present simulations of τ_i were also performed with the widely used GRI Mech3.0 mechanism [6], developed earlier in 1999. This comprises 325 elementary chemical reactions, with related reaction rate constants and the thermodynamic parameters of 53 species. GRI Mech3.0 [6] has improved kinetics and broader target data when compared to the earlier versions of this mechanism. It has been validated for CH_4 and natural gas flame speeds and shock tube measurements between 0.001-1.01 MPa and 1000-2500 K [13].

The simulations were zero dimensional, adiabatic, and at constant volume. The time steps were adaptive, dependent upon P and T, with sufficiently small time meshes of 1.0×10^{-7}-1.0×10^{-10} s for, τ_i, and of $1.0 \times 10^{-12} - 1.0 \times 10^{-14}$ s for τ_e, to ensure grid independent solutions. The nonreacting mixture was compressed instantaneously to P and T at time zero, and τ_i is defined as the period of time between this instant and the onset of the maximum heat release rate. Following Lutz et al. [2], the excitation time, τ_e, is defined as the time from the point where the heat release rate is 5% of the maximum heat release rate to the instant where that maximum value is attained. No experimental validation of the computed values of τ_e is possible, as it is not possible to measure either compositional or temperature changes on such a small time scale. This implies a degree of uncertainty in the controlling chemistry and its applications. To ensure high accuracy of the computed heat release at this lower bound, the value of the heat release was interpolated using cubic splines.

2.2 Reduced global scheme

The global model, outlined in Table 1, is expressed in more detail, with the reduced species reactions, and the overall energy equation given in Table 2. The global reaction rate parameters are of the Arrhenius form:

$$k_n = A_n exp(-[E/R]_n.[1/T]) \tag{Eq. 1}$$

where n is the reaction number, given in Table 1.

The same values were employed initially in the computations of both τ_i and τ_e. The global reaction equation parameters, A, E/R, and H_o, the heat of reaction, for the energy equation, all listed in Table 3, were adjusted to generate values of τ_i as close as possible to those from the detailed kinetic mechanism, using the comprehensive Cantera code and the Mech_56.54 kinetic scheme. Table 3 lists these optimised values of A and E/R for $\phi = 1.0$, that were employed in the G1 Model throughout a regime extending from 4 to 10 MPa, and 700 to 1400 K, relevant to turbocharged engines and gas turbines.

Table 2. Species reactions and energy equation.

Fuel	$d[F]/dt = -k_1[F] - k_3[F][O_2][M] + k_{3R}[I] - 0.5\,k_5[O_2][Y]$	(1)
Oxygen	$d[O_2]/dt = -ak_2[O_2][X][M] - 2\,k_3[F][O_2][M] + 2\,k_{3R}[I]$ $- (a-1)k_5[O_2][Y]$	(2)
Chain Propagating Intermediate	$d[Y]/dt = 2\,k_4[I] - k_5[O_2][Y]$	(3)
Oxygenated Radicals	$d[I]/dt = k_3[F][O_2][M] - k_{3R}[I]$	(4)
Chain Branching Intermediate	$d[X]/dt = k_1[F] - k_2[O_2][X][M]$	(5)
Product	$d[P]/dt = k_2[O_2][X][M] + k_5[O_2][Y]$	(6)
Energy Equation	$dE/dt = (H_1 k_1[F]) - (H_2 k_2[O_2][X][M])$ $- (H_3 k_3[F][O_2][M]) - (H_{3r} k_{3R}[I])$ $- (H_4 k_4[I]) - (H_5 k_5[O_2][Y])$	(7)

Table 3. Reaction rate controlling parameters for G1 Global Model.

Reaction Constant	Rate	A (mol m^3 s)	E/R (K)	H_0 (kJ/mol)
k_1		4.10^7	18050	709.9
k_2		2.10^7	7200	-4709.9
k_3		3.10^6	20000	-100
k_{3R}		3.10^{23}	37500	100
k_4		2.10^7	5000	-60
k_5		5.10^7	16500	-3920

Temporal computational increments of time steps for both τ_i and τ_e were refined until they gave grid independent solutions. These were 1.0×10^{-5} s for τ_i, and 1.0×10^{-9} s for τ_e. The fuel concentration, [F], was a convenient marker and an optimal indicator for both the ignition delay and excitation times, marked by instantaneous acceleration in [F] consumption. From [14], the generalised species, X, were attributed to radicals such as H, and CH_2 as well as ethylene, C_2H_4, while I, was attributed to HO_2, CH_2 and H_2O. Y was attributed to OH, but, as shown in [10], a more accurate description of Y would include further intermediates.

As will be shown, the data in Table 2 were successful in modelling τ_i over a wide range of conditions in the G1 global model. Not surprisingly, when these optimal data were used in an attempt to model τ_e, it failed. Completely new numerical values for the reaction rate parameters, in two sets, one with lower heat release during preignition, more similar to that of the comprehensive scheme for τ_i, and one for τ_e with a much more rapid heat release, were manually adjusted to reflect large differences in heat release rates between τ_i and τ_e reaction stages, in an attempt to model both τ_i and τ_e. The change in heat release needed to reproduce τ_e, while maintaining the overall heat release, also necessitated large changes to reaction rate parameters. These comprised the G2 global model, the numerical values for which are given in Table 4. Initially, G2 was operated with just the first parameter set, that intended for τ_i. Subsequently, upon detection of the initiation of ignition through thresholding of the fuel species concentration [F], the parameter sets were switched. The parameter set intended for τ_i was deactivated and that for the τ_e parameter employed for the remaining reactions.

Table 4. Reaction rate controlling parameters for G2 Global Model.

	Reaction Rate Constant	A (mol m^3 s)	E/R (K)	H$_0$ (kJ/mol)
τ_i	k_1	2.0×10^8	19050	0.05
	k_2	2.0×10^8	7200	-99
	k_3	5.0×10^6	20000	-0.025
	k_{3R}	6.0×10^{21}	37500	0.025
	k_4	4.0×10^6	5000	-0.025
	k_5	1.0×10^7	16500	-99
	Reaction Rate Constant	A (mol m^3 s)	E/R (K)	H$_0$ (kJ/mol)
τ_e	k_1	1.05×10^{10}	21050	1000
	k_2	1.05×10^{10}	8600	-10000
	k_3	6.0×10^9	20000	-1000
	k_{3R}	3.0×10^{20}	36500	1000
	k_4	7.0×10^9	5000	1000
	k_5	7.0×10^9	16500	-8000

3. Computed Values of τ_i from Comprehensive and Reduced Schemes

Figs. 1 (a) and (b) compare the modelled ignition delay times, using both the Mech_56.54 and GRI Mech3.0 detailed kinetic mechanisms with available experimental data from the literature, at different T, for stoichiometric CH$_4$/air, at pressures of 0.1 MPa and 4 MPa, respectively. The plots suggest a near Arrhenius relationship between 1000 and 1800 K. In Fig. 1 (a) agreement between these models and the experimental measurements of Hu et al. [15], Herzler and Naumann [16], Trevino and Mendez [17], and Zeng et al. [18] is satisfactory at the higher temperatures. However, at the lower temperatures the GRI Mech3.0 mechanism tends to overpredict reactivity. The earlier values of Lutz et al. [2] tend to underestimate τ_i to a greater extent than GRI Mech3.0.
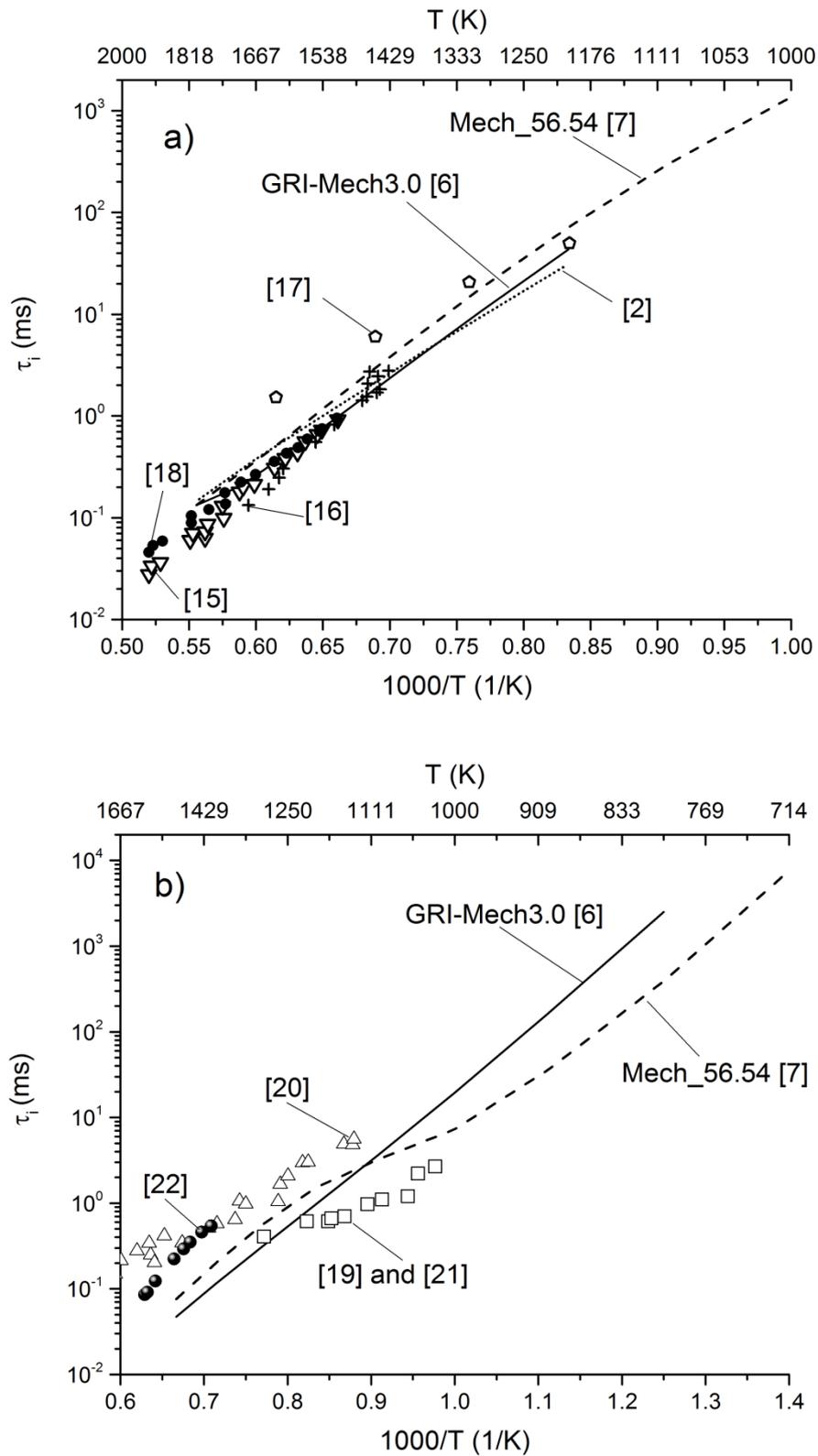
Figure 1. Ignition delay time predictions using both detailed schemes, GRI Mech3.0 [6] and Mech_54.54 [7], and comparison with measured values (a) at 0.1 MPa and (b) at 4 MPa. Lines represent modelled results, symbols referenced experimental data.

There is a much greater scatter in the experimental measurements at the higher pressures in Fig. 1 (b). Both mechanisms show significant differences with the experimental measurements of Huang and Bushe [19], Kim et al. [20], Huang et al. [21] and Merhubi et al. [22]. The Mech_56.54 mechanism tends to capture the overall trend of τ_i variations better than those of the GRI Mech3.0 model, particularly at the lower temperatures. Mech_56.54 has been validated against a rather broader range of pressures and temperatures than GRI Mech3.0. GRI Mech3.0 has been optimised only up to 1.01 MPa. The Mech_56.54 mechanism was therefore employed in the current modelling of τ_i and τ_e. Nevertheless, a severe limitation is that the selected detailed chemistry essentially rests upon shock tube and RCM data that exhibit significant scatter.

The upper curves in Figs. 2 to 4 show the computed values of τ_i for the detailed and both global models, G1 and G2, for stoichiometric CH_4/air, plotted against 1000 K/T at pressures of 4, 6, and 10 MPa, respectively. There is a good agreement between the three sets of values, which are within the bounds of the experimental scatter that is evident in Fig. 1. Agreement is least satisfactory at the lowest temperatures. The ignition delay times vary by about five orders of magnitude over the full range of temperature at all pressures, and by no more than one order of magnitude over the full range of pressures at fixed temperature.
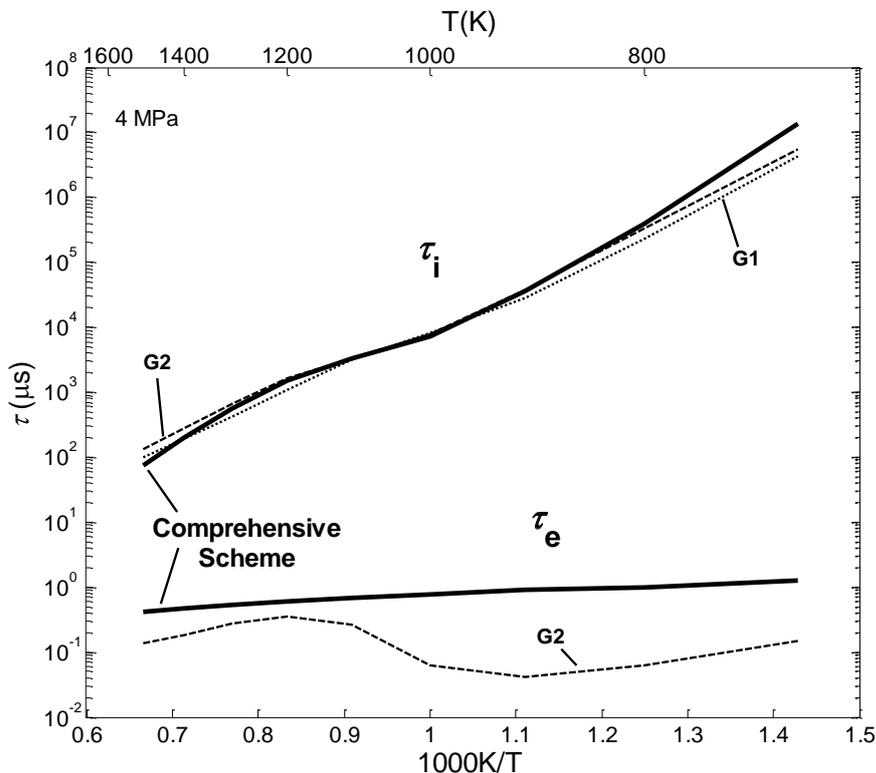

Figure 2. Comparison of ignition delay times, τ_i, and excitation times, τ_e, predicted by Comprehensive and Global schemes, G1 and G2, for stoichiometric CH_4/air at 4 MPa.

Figure 3. Comparison of ignition delay times, τ_i, and excitation times, τ_e, predicted by Comprehensive and Global schemes, G1 and G2, for stoichiometric CH_4/air at 6 MPa.
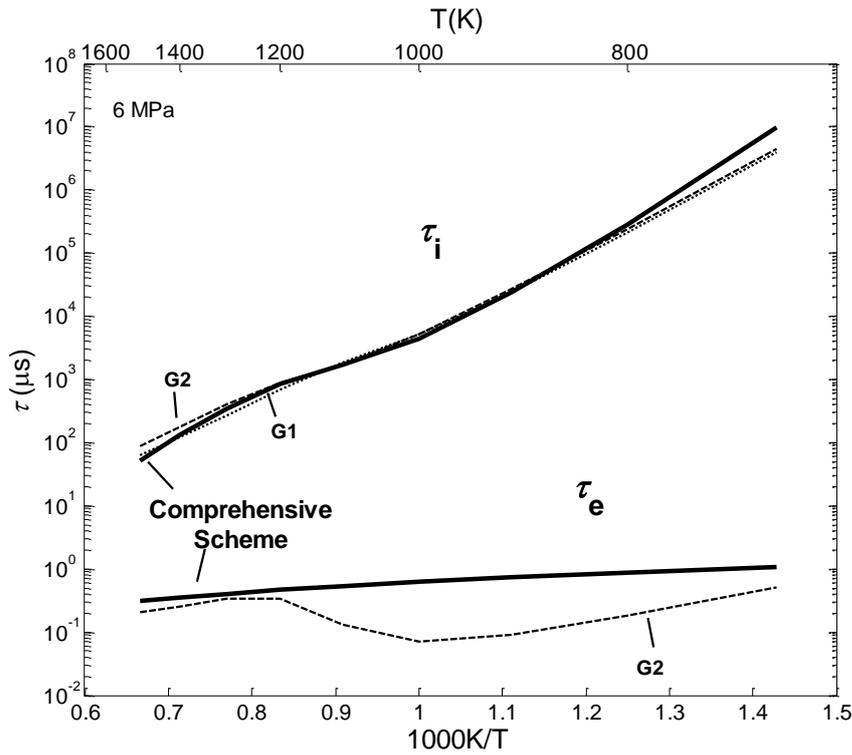

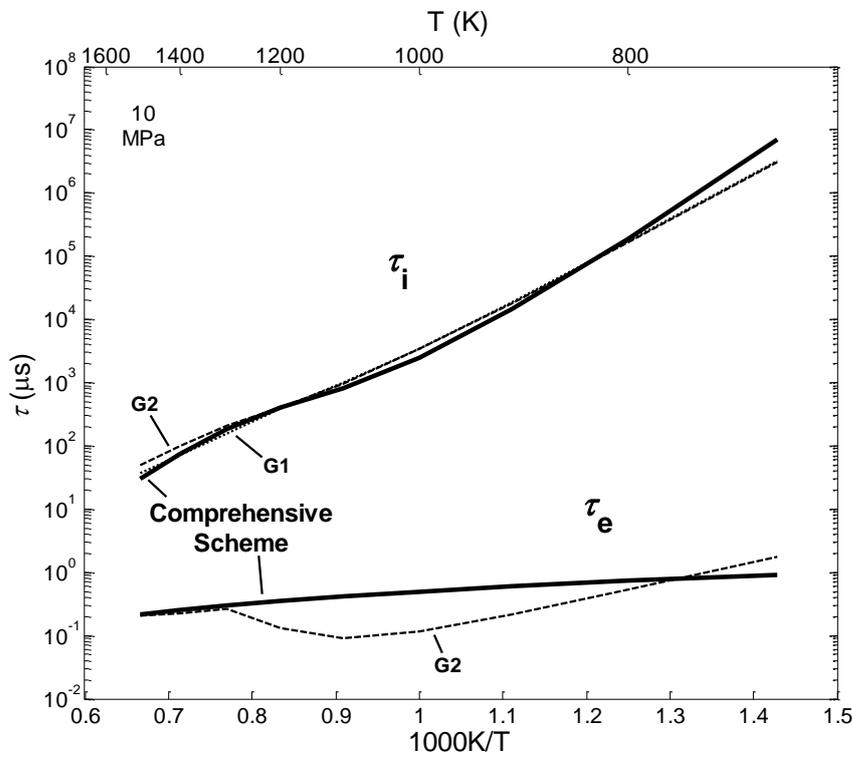
Figure 4. Comparison of ignition delay times, τ_i, and excitation times, τ_e, predicted by Comprehensive and Global schemes, G1 and G2, for stoichiometric CH_4/air at 10 MPa.

4. Computed Heat Release Rates and Excitation Times from Comprehensive and Reduced Schemes
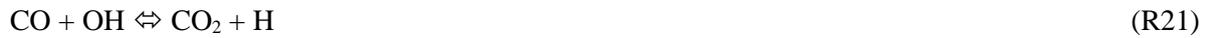
4.1 Comprehensive kinetic scheme computations

During the ignition delay time, chain branching reactions are active with small heat release, yet this period is terminated by the onset of a high heat release rate. The overall volumetric heat release rate, VHRR, is the net thermal energy release rate encompassing all 710 reactions. It has been used in calculating τ_e and has been analysed to determine the principal 23 contributory exothermic and endothermic reactions at different pressures listed in Table 5. These are given for three different values of P and two of T in Table 5. The order in which the reactions appear approximately follows the chronology of the reactions from start to finish. They are selected on the criterion that, during the period within which the total heat release rate is more than 5% of the maximum heat release rate, the reaction should contribute more than 5% of the total. The four most endothermic reactions were selected on a similar basis, within the same regime. The bracketed figures within the Table express the order of increasing endothermicity of the 710 reactions. Numbering is consecutive from 1 to 710, in increasing order of endothermicity. These numbers are given in brackets for each listed reaction. Percentage contributions to the maximum VHRR at the time of this maximum heat release are also given.

Table 5. The 23 principal exothermic and endothermic reactions contributing to the overall Volumetric Heat Release Rate.

No.	Key Reaction	0.1 MPa 1200 K		4 MPa 800 K		4 MPa 1200 K		10 MPa 1200 K	
R1	$CH_4 + OH \Leftrightarrow CH_3 + H_2O$	2.826 %	(12)	0.966 %	(21)	2.077%	(18)	1.597 %	(20)
R2	$CH_3 + H\ (+M) \Leftrightarrow CH_4\ (+M)$	2.640 %	(14)	1.887 %	(14)	4.923 %	(9)	3.058 %	(12)
R3	$CH_3 + O \Leftrightarrow CH_2O + H$	22.346 %	(1)	2.477 %	(10)	6.908 %	(6)	3.531 %	(11)
R4	$CH_2O + H \Leftrightarrow H_2 + HCO$	6.655 %	(5)	1.223 %	(18)	2.997 %	(15)	1.957 %	(16)
R5	$HCO + M \Leftrightarrow CO + H + M$	-10.395 %	(709)	-3.298 %	(708)	-6.605 %	(709)	-5.072 %	(709)
R6	$CH_2 + O_2 \Leftrightarrow HCO + OH$	6.739 %	(4)	1.485 %	(16)	3.293 %	(14)	2.227 %	(14)
R7	$HCO + O_2 \Leftrightarrow CO + HO_2$	1.794 %	(25)	0.313 %	(39)	0.588 %	(35)	0.395 %	(40)
R8	$CH_3OH\ (+M) \Leftrightarrow CH_3 + OH\ (+M)$	0.522 %	(43)	3.005 %	(9)	4.185 %	(12)	4.533 %	(9)
R9	$H + O_2 \Leftrightarrow O + OH$	-22.190 %	(710)	-14.819%	(710)	-17.191 %	(710)	-13.682 %	(710)
R10	$2CH_3\ (+M) \Leftrightarrow C_2H_6\ (+M)$	0.151 %	(71)	0.011 %	(114)	0.068 %	(92)	0.034 %	(98)
R11	$C_2H_4 + H\ (+M) \Leftrightarrow C_2H_5\ (+M)$	-0.209 %	(699)	-0.011 %	(687)	-0.067 %	(691)	-0.037 %	(690)
R12	$H + O + M \Leftrightarrow OH + M$	0.092 %	(89)	2.403 %	(11)	1.725 %	(21)	2.183 %	(15)
R13	$H + HO_2 \Leftrightarrow 2OH$	3.606 %	(10)	5.495 %	(7)	5.165 %	(8)	5.231 %	(7)
R14	$H_2O + O \Leftrightarrow 2OH$	-0.988 %	(707)	-4.535 %	(709)	-2.672 %	(708)	-3.149 %	(708)
R15	$H + HCO \Leftrightarrow CO + H_2$	5.728 %	(6)	0.425 %	(34)	1.207 %	(27)	0.567 %	(33)
R16	$H + O_2\ (+M) \Leftrightarrow HO_2\ (+M)$	0.225 %	(63)	17.995 %	(2)	10.104 %	(2)	14.530 %	(2)
R17	$2HO_2 \Leftrightarrow H_2O_2 + O_2$	0.032 %	(121)	0.388 %	(35)	0.245 %	(53)	0.577 %	(31)
R18	$HCCO + O_2 => CO + CO_2 + H$	0.989 %	(31)	0.549 %	(29)	0.709 %	(32)	0.585 %	(30)
R19	$HCCO + OH => 2CO + H_2$	7.972 %	(3)	5.509 %	(6)	7.403 %	(5)	5.597 %	(6)
R20	$H_2 + OH \Leftrightarrow H + H_2O$	12.076 %	(2)	6.978 %	(5)	8.813 %	(3)	7.275 %	(5)
R21	$CO + OH \Leftrightarrow CO_2 + H$	4.562 %	(6)	14.605 %	(3)	7.847 %	(4)	8.934 %	(4)
R22	$H + OH + M \Leftrightarrow H_2O + M$	0.592 %	(39)	23.195 %	(1)	13.768 %	(1)	20.824 %	(1)
R23	$HO_2 + OH \Leftrightarrow H_2O + O_2$	2.339 %	(18)	10.950 %	(4)	6.550 %	(7)	8.968 %	(3)

At 4 and 10 MPa the principal reactions contributing to the heat release rate are:

$$H + OH + M \Leftrightarrow H_2O + M, \tag{R22}$$

$$CO + OH \Leftrightarrow CO_2 + H \tag{R21}$$

or

$$H + O_2 (+ M) \Leftrightarrow HO_2 (+ M) \tag{R16}$$

with

$$HO_2 + OH \Leftrightarrow H_2O + O_2 \tag{R23}$$

and

$$H_2 + OH \Leftrightarrow H + H_2O. \tag{R20}$$

Not surprisingly, these are predominantly termination reactions, whereas previous work has shown that the time to ignition for CH_4/air mixtures is highly sensitive to chain branching routes such as R24 and R9 [7, 23, 24]:

$$CH_3 + O_2 \Leftrightarrow CH_2O + OH, \text{ and} \tag{R24}$$

$$H + O_2 \Leftrightarrow OH + O. \tag{R9}$$

However, Nagy et al. [25] noted a high degree of uncertainty concerning R22, especially at high temperatures [26]. Experimental data points in support of a particular value of rate coefficient are sparse. Potential inconsistencies also occur in the data for R23, in that Burke et al. [27] suggested a temperature dependence different from that in [26]. In addition, R23 has been shown by Burke et al. [7] to have a weak sensitivity for the simulation of CH_4 ignition delays at high pressure, and to inhibit ignition, as does R16.

Along with R21, R20 is an important exothermic contributor at the lower pressure of 0.1 MPa and 1200 K, as shown in Fig. 5. Here it can be seen that the principal contributor to the heat release rate is:

$$CH_3 + O \Leftrightarrow CH_2O + H. \tag{R3}$$

At this lower pressure, R22 and R16 seem to be unimportant, contributing less than 1 % of the overall heat release compared to higher pressure conditions. This is because the rates of these reactions increase with pressure due to third body effects. The principal contributors are now R3 and R20. According to Nagy et al. [25] R20 also has a high sensitivity to the calculated burning velocities for hydrogen and syngas systems at fuel lean conditions. Varga et al. [26] optimised the rate coefficients for this reaction and showed very small uncertainty in the predictions of this reaction, which are very close to the experimental data. Consequently, there is a high degree of confidence in the value of the rate coefficient

in this reaction. We might therefore anticipate a higher degree of uncertainty in predicting heat release rates at high pressures than at low pressures.

The contributions of each of the principal reactions to the overall VHRR are compared in Fig. 5 and 6. These are, respectively, for 0.1 and 10 MPa, the lowest and highest pressures studied. An unshaded rectangle is indicative of this percentage at the time for the first 5% of the maximum total VHRR, a black rectangle at the time of the maximum total VHRR, and a shaded rectangle at the time of the last 5% of the maximum total VHRR.
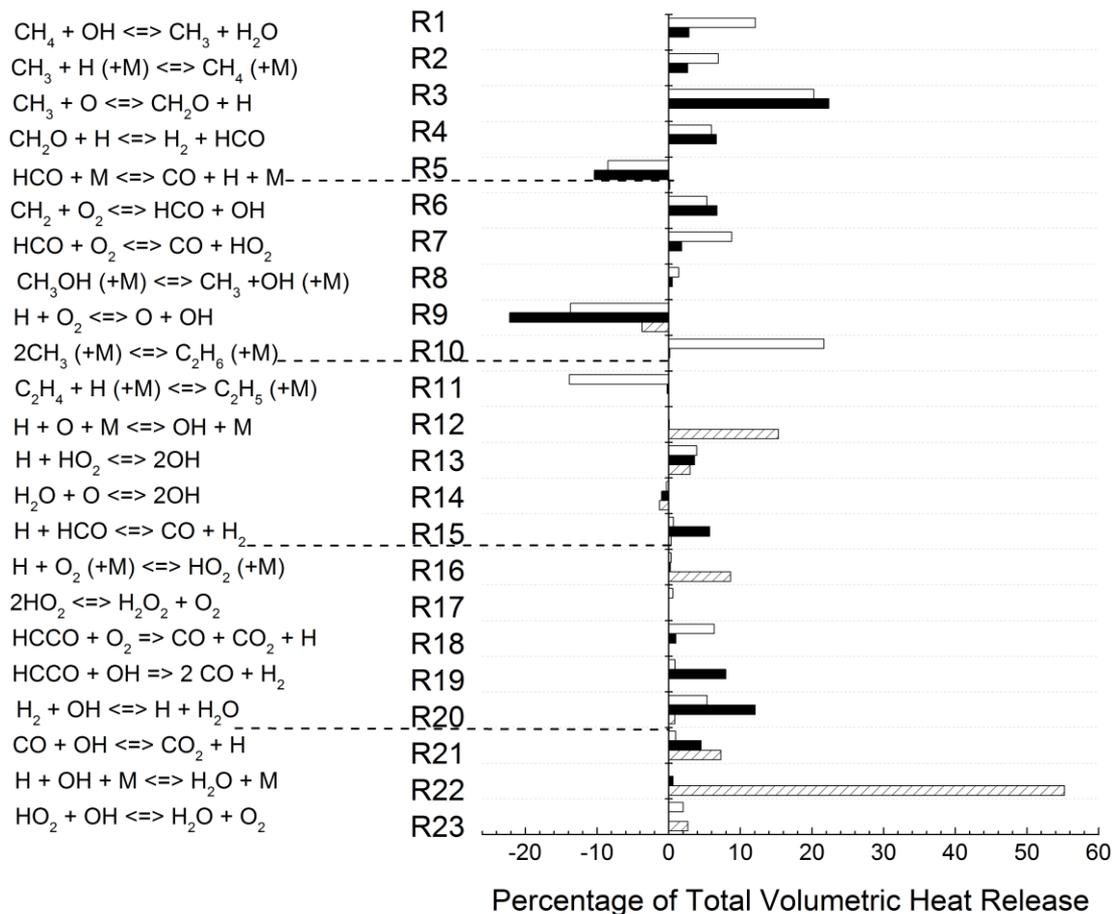

Figure 5. Principal reactions contributing to volumetric heat release rate, VHRR, with Mech 56.54 [7], P=0.1 MPa and T=1200 K. Black fill indicates VHRR of the reaction at the point of maximum total VHRR. No fill indicates contribution at a VHRR of the reaction that is 5% of this maximum, during the increase in VHRR. Shaded fill indicates contribution at a VHRR that is 5% of the maximum total VHRR, during the decrease of VHRR.
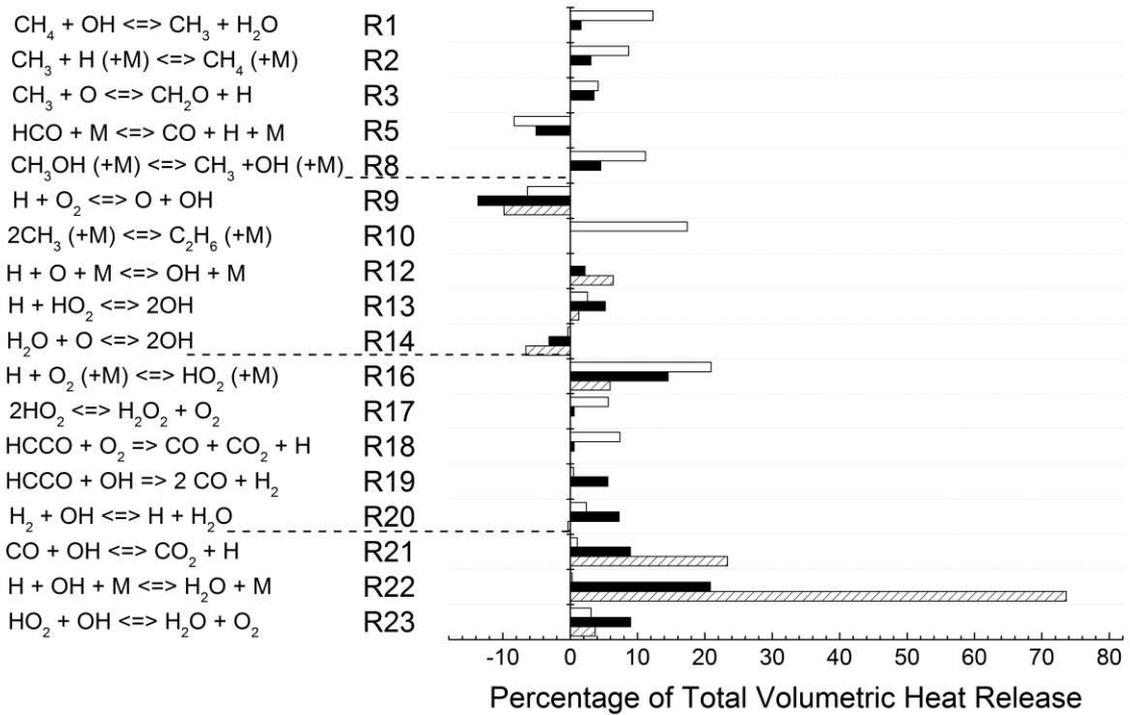
Figure 6. Principal reactions contributing to volumetric heat release rate, VHRR, for Mech 56.54 [7] at P=10 MPa and T=1200 K. See Fig. 5 caption for key to rectangle fills.

More detailed temporal distributions, of the volumetric total VHRR, at initial pressures of 0.1, 4 and 10 MPa, are shown by the bold dashed curves in Figs. 7 to 10. Other profiles on these figures are for the four principal exothermic and one endothermic reaction that contribute to this overall rate. In these cases the profiles are only shown at some selected instants. Fig. 8 also shows the typically good correspondence that was found to exist between the volumetric heat release rate and the pressure gradient.

16

Figure 7. Mech 56.54 [7] heat release profiles for largest contributing reactions to total heat release at P=0.1 MPa and T=1200 K.

Figure 8. a) Mech 56.54 [7] heat release profiles for largest contributing reactions to total heat release at P=4 MPa and T= 800 K and b) the pressure gradient.
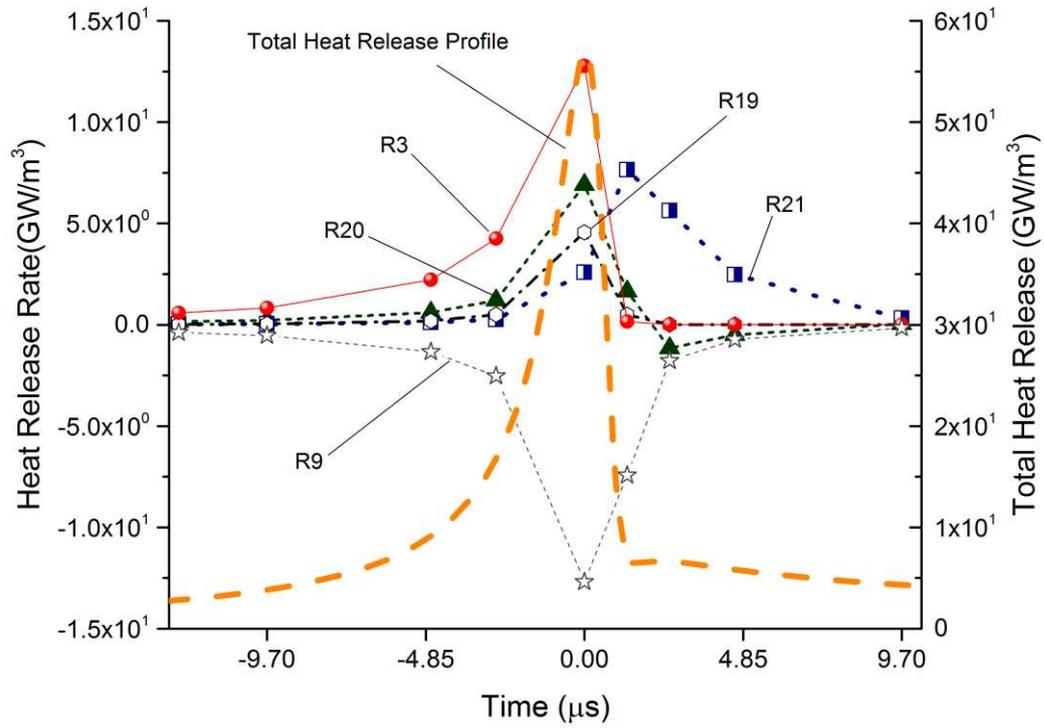
Figure 9. Mech 56.54 [7] heat release profiles for largest contributing reactions to total heat release at P=4 MPa and T=1200 K.
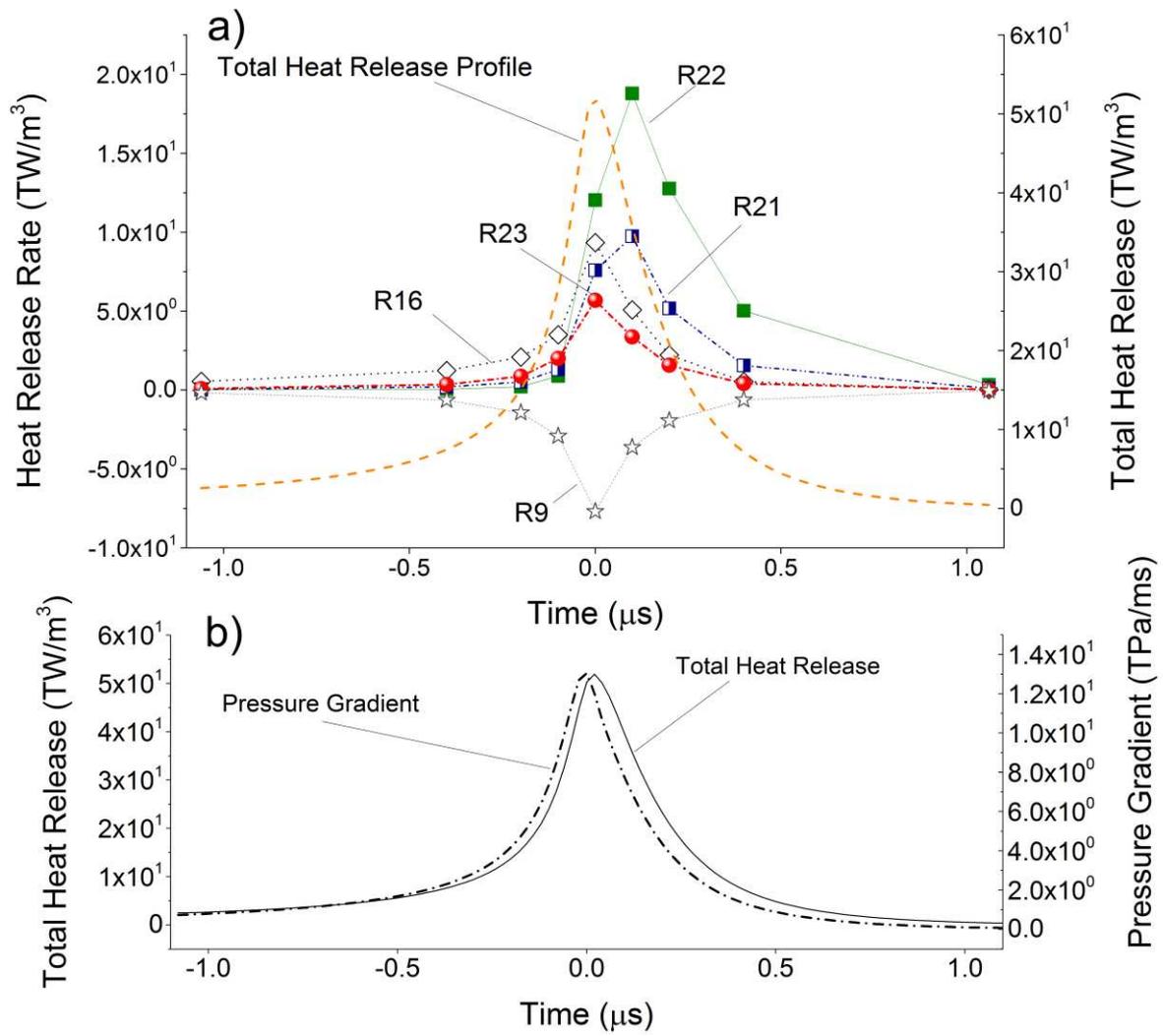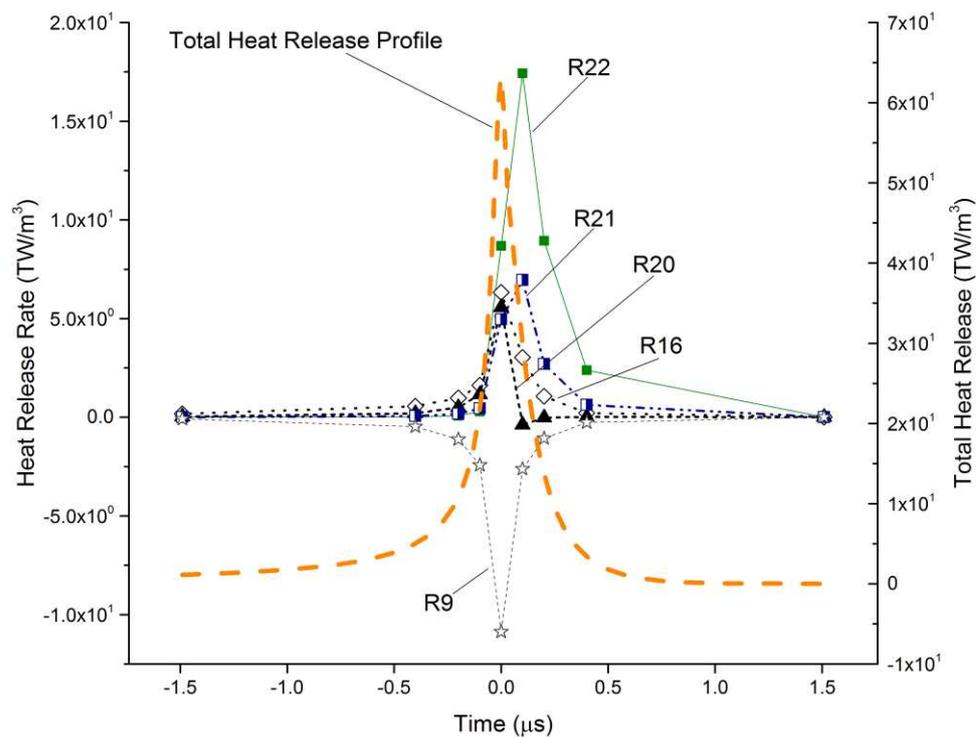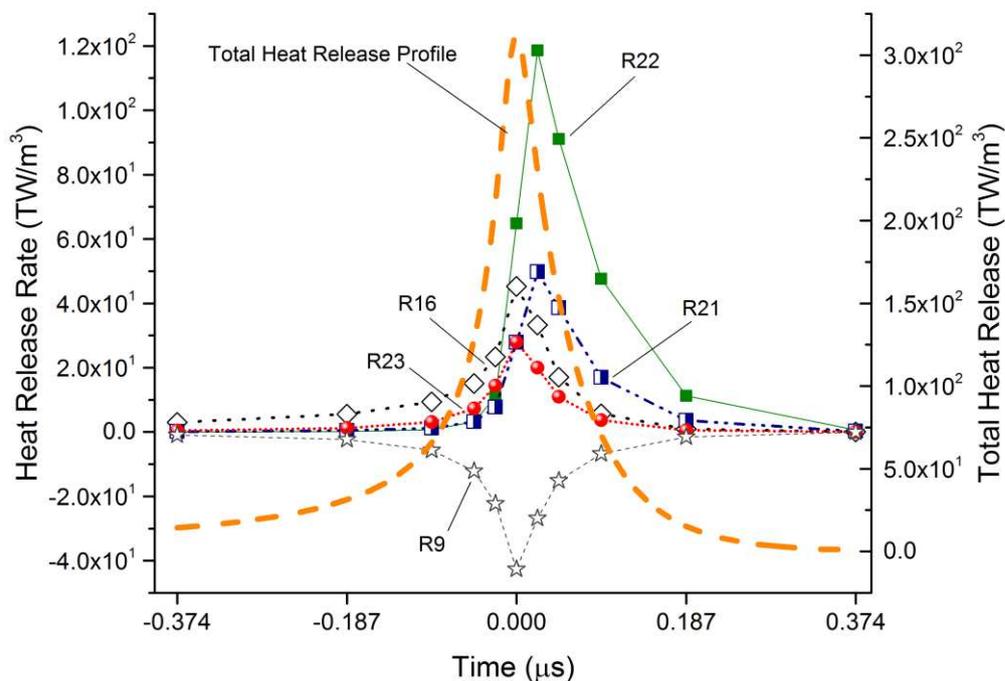

Figure 10. Mech 56.54 [7] heat release profiles for largest contributing reactions to total heat release P=10 MPa and T=1200 K.

The temporal profiles of the VHRR, at 4MPa and 1200K, are employed in Fig. 11, to demonstrate the defined value of τ_e, extending from 5% of the maximum heat release rate to the maximum value [2]. The heat release rate profile also suggests a possible alternative definition of τ_e, as the period of time during which the heat release rate is more than, say, 20% of the maximum, as also indicated on Fig. 11. This definition might be a better choice of τ_e, since during this time the most intense heat release is fed into the acoustic wave.
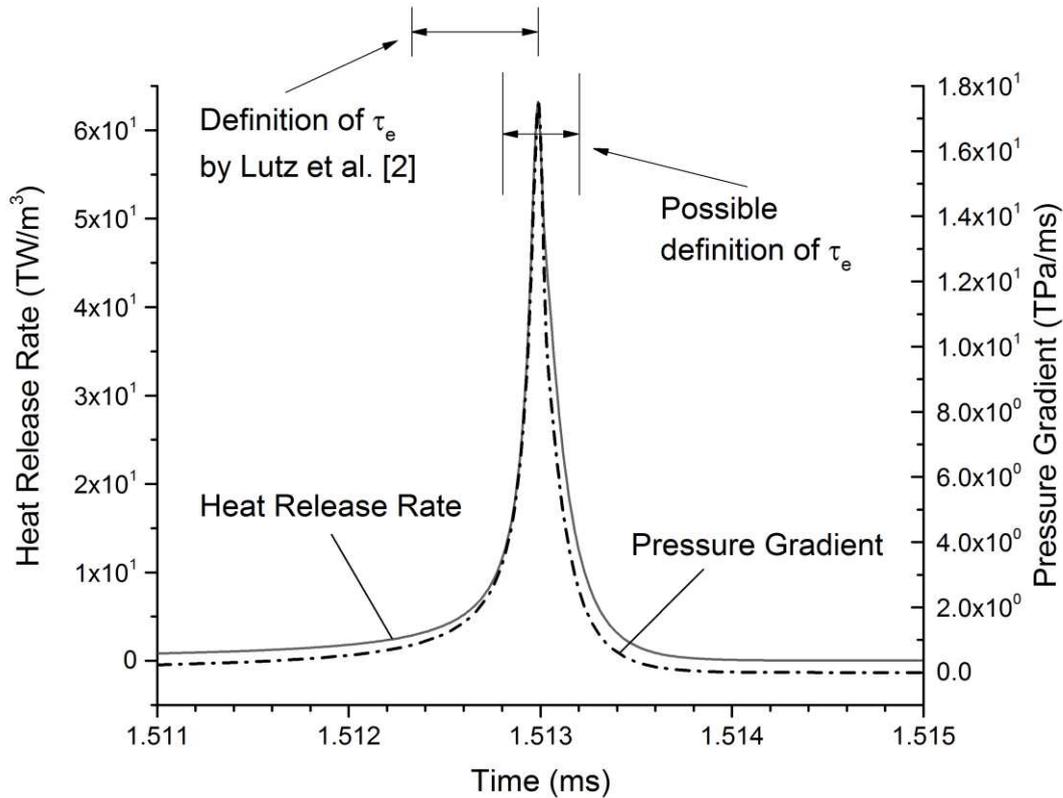
Figure 11. Volumetric heat release rates, at times after the instantaneous compression of a stoichiometric CH_4/air mixture at initial P= 4 MPa and T = 1200 K.

4.2 Reduced global scheme computations

Although the reduced global G1 model was able to generate sufficiently accurate values of τ_i, close to those of the comprehensive scheme, not surprisingly, the same cannot be said of the values of τ_e. Despite the employment of sufficiently small time increments in the computations of τ_e, the computed values, from the same global reaction parameters as for τ_i, were several orders of magnitude greater than those from the comprehensive scheme.

20

The large differences in τ_e between the two schemes are manifest also in the differences in the computed volumetric heat release rates. The comprehensive scheme shows relatively little heat release during the preignition period, followed by a rapid increase in heat release rate in a narrow pulse. In contrast, the reduced global G1 scheme has significantly more heat release during the preignition period, with a more gradually increasing rate towards the end of the preignition period and into the τ_e zone.

Both sets of these G2 global equations parameter values are given in Table 4. The numerical values in the two sets are very different, as they are also when compared with those of the G1 scheme in Table 3. The two set approach necessitates much higher heats of reaction for the computation of τ_e. In contrast, for the computation of τ_i the heats of reaction were chosen to give very little heat release over the preignition period, lower than those employed in the G1 scheme. This necessitated higher reaction rate parameters for the G2 scheme. For both data sets the aims were to approach the predictions of τ_i, and τ_e, given by the comprehensive scheme, as closely as possible.

The resulting predictions using the G2 scheme are shown in Figs. 2 to 4. It can be seen that the G2 predictions of τ_i are close to those of the G1 scheme, but with a tendency to overpredict at the higher temperatures. Unlike the G1 scheme, the G2 scheme was capable of giving reasonable predictions of τ_e, although these were generally underpredicted by up to almost an order of magnitude. However, the general trend with varying temperature was to follow the predictions of the comprehensive scheme.

5. Discussion

5.1 Comprehensive chemical kinetic and global reaction schemes

The key reactions discussed in Section 4.1 at the time of maximum VHRR are more dependent upon pressure than temperature. Interestingly, immediately after the time at which the heat release rate is a maximum, the principal contributors to the overall heat release rate are the same for all the four conditions studied, but in slightly varying orders of magnitude, R22, R21, R16 and R12. The high pressure conditions of 4 and 10 MPa produce large contributions from the three body exothermic reactions R22 and R16 during the excitation time. This follows from the stronger dependence of the maximum VHRR on pressure. Since the rate of these reactions cannot attain that of the rapid chain branching at higher temperatures, they peak after the instant of peak VHRR. For the low pressure condition of 0.1 MPa, the exothermic reactions R3 and R20 contribute most to the energy release. Of all the conditions tested, reaction R9 appears to be the main endothermic reaction. The branching reaction, R9, $H + O_2$, is the principal reaction in combustion.

Both the comprehensive chemical kinetic and the global reaction models proved capable of predicting values of τ_i that are sufficiently close to the measured values. However, there are many uncertainties involved in simulations and results are highly dependent on the accuracy of the schemes. This is

particularly so at the highest pressure of 10 MPa, at which there are few, if any, direct measurements of τ_i for stoichiometric CH_4/air. There can be no such practical check on the predicted values of τ_e and the only procedure for its evaluation is through the detailed chemical kinetics route. Not surprisingly, a single set of global rate parameters and heats of reaction were incapable of successfully modelling both τ_i and τ_e. What was surprising, was that when two separate sets of global rate parameters were employed, one for τ_i, and one for, τ_e, in the G2 global model, there were good predictions of τ_i, while those for τ_e were within an order of magnitude of the values obtained from the comprehensive chemical kinetics scheme. While the G1 model presented no problems, the key problems in the overall global optimisation with G2 were keeping the heat release rate, at realistically low values, during the ignition delay time and minimising any tendency towards a negative temperature coefficient during the excitation time

The virtue of the global scheme is its computational speed, an important factor in the modelling of chemically reacting flow, when the flow equations inevitably compete for the computing resource. The reduced global model was able to compute a single τ_i value, using Matlab's ODE15s solver for T = 1000 K and P = 6 MPa within 0.83 seconds. For the computations of τ_e, with a much reduced time mesh, this time was extended to 17.14 seconds. In contrast, the detailed kinetic scheme using Cantera software computed a value of τ_i, within 6.55 seconds and of τ_e, using advanced time step, within 199.69 seconds for the same conditions. The global scheme is significantly less computationally expensive than the comprehensive alternative, but it would require further development to produce sufficiently accurate values of τ_e. Furthermore, in the absence of experimental data for τ_e, the global scheme is dependent on existing comprehensive schemes.

The excitation times calculated with the complete kinetic scheme decrease slightly with increasing temperature and exhibit little change with pressure, a similar trend to that observed in [2]. This is in contrast to the influence of temperature and pressure upon τ_i. The ignition delay times, vary by about five orders of magnitude over the full range of temperature at all pressures, but by no more than one order of magnitude over the full range of pressures at a fixed temperature.

It is of interest to note the very high magnitudes of some of the peak volumetric heat release rates, particularly at high pressures and temperatures. At 0.1 MPa and 1200 K the maximum volumetric heat release rate of 15GW/m**3** is about 2.5 times that of the peak heat release rate in a laminar flame and 75 times that in a gas central heating boiler [28]. What is striking, however, is the very high heat release rate of 120 TW/m^3 at 10 MPa and 1200 K.

5. 2 The Detonation Peninsula and knocking propensity of different fuels

The excitation time is featured in the present work because of the growing awareness of it importance in the transition to detonation and also the stability of detonation waves [29, 30]. It features in an assessment of the knocking tendencies of different fuels. It is not based on Octane Numbers, which are a somewhat limited guide for the assessment of modern engines operating at higher pressures with new fuels [31]. Knock originates when the rate of change of the heat release rate at a hot spot generates a significant pressure pulse. The time for the pressure wave to traverse the hot spot, is the hot spot radius, r, divided by the acoustic velocity, a. The ratio of this time to the excitation time, gives the value of ε, a measure of the reinforcement of the pressure pulse by the heat release. Another dimensionless group, ξ, comprises a, normalised by the autoignitive propagation velocity, u_a, equal to $dr/d\bar{\tau_i}$. Values of ξ, when plotted against ε at the limit for hot spot autoignitions that lead to developing detonations, create a detonation peninsula. Within it, detonations can develop [4, 29]. This is shown on the ξ/ε diagram in Fig. 12, from an earlier study of autoignition in engines [32].
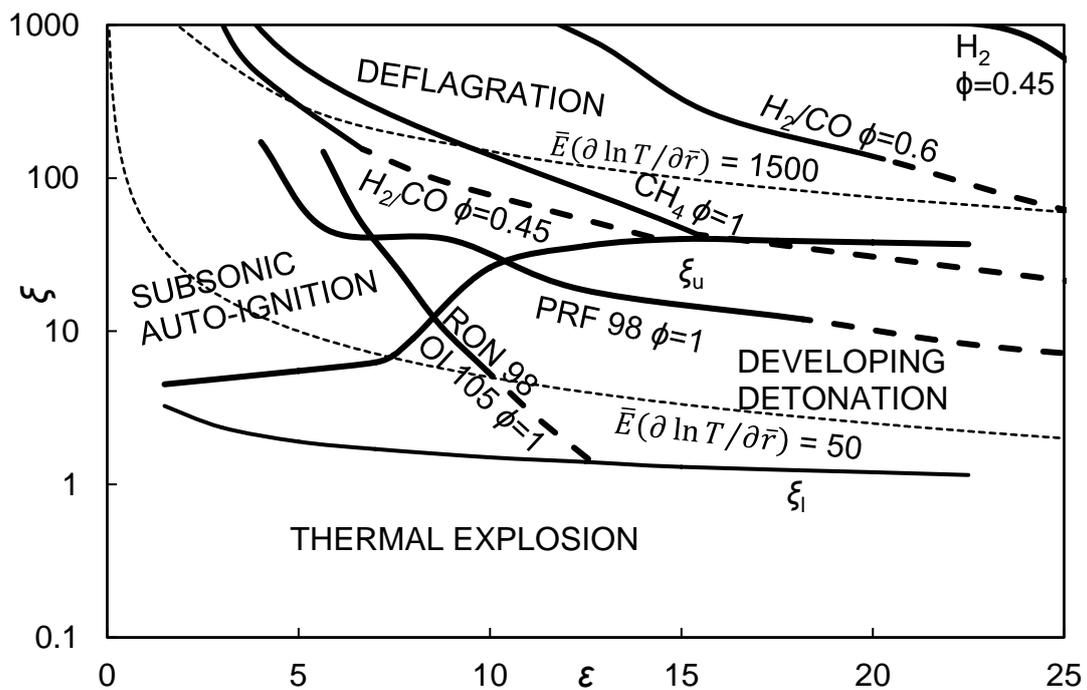
Figure 12. Isentropic compression curves for different fuels showing propensity for detonation. Solid curves indicate compression from 800 K to 1000 K at ≈10 MPa. Broken curves show continuation of this compression to 1100 K at 15 MPa, relevant to turbo charged engines.

Loci of engine compressions for six different fuel/air mixtures, including CH_4/air, at different equivalence ratios, ϕ, are also shown. Compressions of the mixtures are downwards toward the peninsula, first with an increasing propensity to engine knock, and, within the peninsula, increasing

knock severity. This increases with increasing penetration into the toe of the peninsula and increasing ε. It decreases in the thermal explosion regime [33].

The solid line isentropes are compressions to 800 K and 10 MPa. The continuing dashed isentropes are compressions to 15 MPa and 1100 K, representing conditions that might occur in turbocharged engines. The H_2 and H_2/CO isentropes do not cross the upper limit of the detonation peninsula and there is no detonation. Those for the two gasolines, one with a Research Octane Number, RON, of 98, the other a Primary Reference Fuel, PRF98, enter the peninsula in the first compression stage. There they remain and detonate at hot spots, with increasingly severe engine knock as the curves penetrate further into the peninsula.

The CH_4/air $\phi = 1.0$, isentrope does not even enter the detonation peninsula during the first stage of compression to 10 MPa. This only occurs during the subsequent compression to 15 MPa. Then, it only skirts along the upper limit of the peninsula, indicating the relatively strong resistance to knock of CH_4/air. The CH_4/air mixtures are characterised by relatively high values of both E/R and τ_i/τ_e, while the gasoline fuels are associated with lower values of E/R.

The ξ/ε diagram in Fig. 12 also shows contours of $\overline{E}\left(\partial \ln T / \partial \bar{r}\right)$, which is equal to the product $(\xi \varepsilon)$ [4]. Here E/R is the autoignitive activation temperature for τ_i, $\overline{E} = \left(\tau_i / \tau_e\right)\left(E/RT\right)$, $\left(\partial \ln T / \partial \bar{r}\right)$ is the dimensionless temperature gradient at the hot spot, and r the radius within the hot spot of radius r_o. This term can be approximated by $\ln(T/T_o)$ [4], with T_o the peak temperature at the centre of the hot spot. Values of $\overline{E}\left(\partial \ln T / \partial \bar{r}\right)$ equal to 50 and 1500 are shown by the dotted curves in Fig. 12. Values approach 10 at the strong ignition limit and are conducive to stable detonations, with a uniform reaction zone strongly coupled with the shock wave [29]. Low values of $\overline{E} \ln(T/T_o)$ are associated with the most stable detonations [11, 29]. High values, above a threshold of about 1500, were tentatively suggested in [4] as a regime of increasing deflagration.

5.3 Autoignitive and deflagrative propagation regimes

In the region close to $\overline{E}\left(\partial \ln T / \partial \bar{r}\right) = 1500$, direct numerical simulations, DNS, [34], experimental analysis, [35], and engine performance [32] show both modes of reaction propagation from hot spots can coexist, sometimes in about equal measure. For stoichiometric CH_4/air, values of $\overline{E}$ were calculated at 0.1, 4, 6 and 10 MPa for different temperatures using the computer codes and the data in Figs. 1 to 4. The probable values of $\left(\partial \ln T / \partial \bar{r}\right)$ will be distributed and, consequently, less definite. The experimental RCM studies of Mansfield and Wooldridge [36] of the propagation of reaction in syngas mixtures, with $\phi = 0.5$, showed it became predominantly deflagrative with dT/dr -5 K/mm. More recently, Mansfield et al. [37] employed the Sankaran criterion [34], that defines the autoignitve regime

as that in which the autoignitive propagation velocity is greater than the laminar burning velocity, and showed values of dT/dr of between -5 and -10 K/mm to be in excellent agreement with the measured transitions between the two regimes.

The engine experiments of Kalghatgi et al. [38] suggest a most probable engine temperature gradient of about -2 K/mm. Combined with an often assumed hot spot radius, r_o, of 5 mm, this was used, alomg with the and the calculated values of $\bar{E}$ to give $\bar{E}(\partial \ln T/\partial \bar{r})$ for stoichiometric CH$_4$/air. These values are employed as a function of temperature for the isobars of 0.1, 4, 6 and 10 MPa in Fig. 13. However, there is no clear boundary between the autoignitive and deflagrative regimes, which can coexist within a transition regime, in which there is also uncertainty about the details of hot spot structures. The two distinctive regimes are indicated in the figure, with the hatched transition regime between them. It can be seen that autoignition is favoured by higher pressures and temperatures. As will be shown, experimental evidence suggests a transition regime extending over the hatched limits in Fig.13.

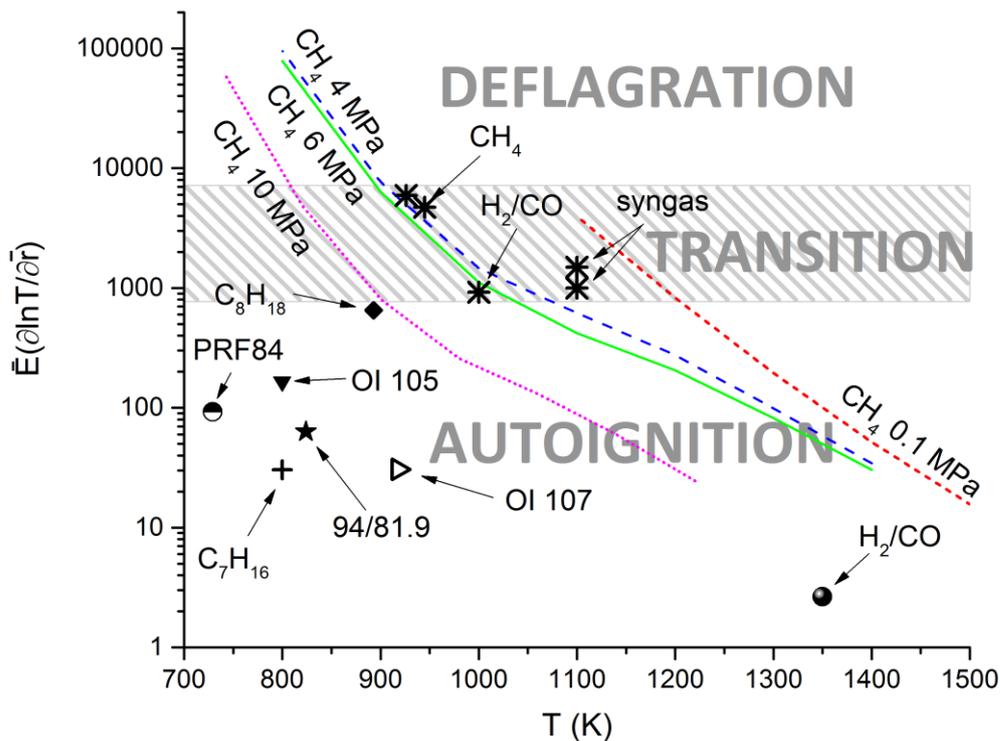

Figure 13. (a) $\bar{E}(\partial \ln T/\partial \bar{r})$ as a function of T and P for stoichiometric CH$_4$/air. (b) Asterisks indicating experimental and computed values of $\bar{E}(\partial \ln T/\partial \bar{r})$ at given T in the transition regime. (c) Engine operational data of different fuels. Details in Table 6. (d) Three regimes of reaction propagation.

The extent of the transition regime for stoichiometric CH_4/air has been studied experimentally by Strozzi et al. [35] at pressures close to 4 MPa in an RCM. They employed both chemiluminescence and planar laser induced fluorescence to visualise the structure of the reacting mixture after compression. It was fond that autoignition was associated with a very rapid rate of pressure rise, that was significantly reduced, with increased deflagrative burning, and an increase in the apparent value of τ_i when the temperature was decreased from 945 K to 926 K. The changes at these temperatures are marked by the two asterisked CH_4 points on Fig. 13, with respective values of $\overline{E}\left(\partial \ln T / \partial \overline{r}\right)$ of 4729 and 5927.

The transition regime studied by Mansfield and Wooldridge [36] employed syngas/air mixtures, see Table 6, with $\phi = 0.5$, became predominantly deflagrative when dT/dr -5 K/mm. With this gradient and assumed values of $r_o = 3$ mm and $\overline{\overline{E}} = 1.1 \times 10^5$ at 1100 K [4], $\overline{E}\left(\partial \ln T / \partial \overline{r}\right)$ was found to be 1490. With the present assumed hot spot characteristics this value becomes 996. Both these estimated transition points are shown by the syngas asterisks on Fig. 13.

Another mixed regime coordinate is provided by the computed τ_i and τ_e data derived in the DNS studies of hot spot autoignitions in (0.5 CO +0.5 H_2)/air mixtures in [39]. For this, the conditions were $\phi = 0.6$, T=1000 K, and P = 5.066 MPa. With the present assumed hot spot conditions this gives $\overline{E}\left(\partial \ln T / \partial \overline{r}\right)$ = 919, marked by the H_2/CO asterisk in Fig. 13. This same study provided another H_2/CO theoretical point is provided in the Fig.13, for 1350 K, P = 5.066 MPa and $\phi = 1.0$, this time in the autoignition regime, well within the detonation peninsula, with $\overline{E}\left(\partial \ln T / \partial \overline{r}\right)$ = 2.64. The upper and lower asterisk points in Fig. 13 are tentatively taken as indicators of the limits of the transition regime.

26

Table 6. Data for plots of $\bar{E}\left(\partial\ln T/\partial\bar{r}\right)$ against temperature at different pressures.

Fuel	Conditions and References	ϕ	P (MPa)	T (K)	10^{-3} $\bar{E}$
CH$_4$	Present computations RCM [4]	1.0	4.0	926	551.78
	Present computations RCM [4]	1.0	4.0	945	449.31
Syngas 0.59H$_2$/0.41 CO/H$_2$/air	RCM [36]	0.5	0.8	1100	110
0.5 H$_2$ + 0.5 CO	Present computations [39]	0.6	5.066	1000	92.34
	Present computations [39]	1.0	5.066	1350	0.358
94RON/81.9MON	Turbocharged engine [4]	1.0	10.45	824	5229
PRF84	Engine running in autoignitive mode [4]	0.25	6.52	729	6.799
OI 107 98 RON/ 89 MON	Turbocharged engine [4]	1.0	13.3	918	2822
OI 105 0.62 ioctane/0.29 toluene/0.09 nheptane 95 RON/ 85 MON	Turbocharged engine, light autoignition [4]	1.0	7.0	800	13.269
C$_8$H$_{18}$	Theoretical [4]			893	58.700
C$_7$H$_{16}$	Theoretical [4]			800	2.450

The data points on Fig. 13 have been extended by the inclusion of existing engine operational data. These are predominantly engine operational points and are in the autoignitive regime. PRF84 was an engine running on a very lean mixture in the autoignitive mode. The different mixtures, of course, would have different isobars. Values of ϕ, P, T, $\bar{E}$, and other details for these points are given in Table 6. The presently assumed hot spot conditions were employed in deriving $\bar{E}\left(\partial\ln T/\partial\bar{r}\right)$. All these data, predominantly based on Primary Reference Fuels and their blends are, not surprisingly, in the autoignitive regime, below the $\bar{E}\left(\partial\ln T/\partial\bar{r}\right) = 1500$ line.

The engine heavy knocking regime is at about $\bar{E}\left(\partial\ln T/\partial\bar{r}\right) = 31$, extending from about 910 to 950 K. It is of interest to note that, while engine operation is impaired by low values of $\bar{E}\left(\partial\ln T/\partial\bar{r}\right)$, measurements of τ_i in RCMs are impaired by high values of this parameter. Values greater than 1500

might result in hot spot initiated autoignitions, from which a laminar flame propagates. This can create erratic apparent values of τ_i, that are inaccurate and usually excessively high.

Conclusions

1. Detailed chemical kinetics, using the Mech_56.54 mechanism and a reduced global reaction scheme, have been used to compute τ_i as a function of P and T. Both schemes, the latter when suitably tuned, are able to calculate values of these parameters over a large range, which lies within the uncertainty bounds of the experimental measurements.

2. The values of τ_e that are presented are essentially only those of the chemical kinetic model. In the absence of any experimental data to calibrate the global scheme, any assessment of its capabilities can only be in terms of the predictions of the detailed chemical kinetic model. Although the G2 global model yields values of τ_e that follow the same trends as the predictions using the detailed scheme over the same range of P and T, they are underpredicted within an order of magnitude.

3. Calculations of τ_e require much smaller time increments than those for τ_i by about five orders of magnitude for the chemical kinetic model, and four orders for the global model.

4. Calculations of both τ_i and τ_e were about 10 times faster with the reduced global mechanism.

5. The four reactions that contribute most to the overall heat release rate have been identified for the different values of P and T, along with the two principal endothermic reactions. These are rather different at atmospheric pressure compared to higher pressures. There is a greater degree of uncertainty in the reaction rates at the highest pressure.

6. At 10 MPa and 1200 K the computed maximum volumetric heat release rate was 120 TW/m^3.

7. The very good antiknock properties of stoichiometric CH_4/air, in comparison with those of other fuels, under turbocharged engine running conditions, have been demonstrated on the ξ/ε diagram.

8. Both τ_i and τ_e data have been employed in attempts to identify the extent of the transition regime between those of autoignitive and deflagrative propagation, in terms of the $\overline{E}\left(\partial \ln T / \partial \overline{r}\right)$ parameter.

9. Rapid compression machines should operate within the autoignitive regime.

Acknowledgements

References

1.   D. Bradley, M. Lawes, M. Materego, Interpretation of auto-ignition delay times measured in different rapid compression machines, Proc. 25th International Colloquium on the Dynamics of Explosions and Reactive Systems, Leeds, UK (2015).

2.   A. E. Lutz, R. J. Kee, J. A. Miller, H. A. Dwyer, A. K. Oppenheim, Dynamic effects of autoignition centers for hydrogen and C1, 2-hydrocarbon fuels, Symp. (Int.) Combust. 22 (1989) 1683-1693.

3.   J. W. Meyer, L. M. Cohen, A. K. Oppenheim, Study of exothermic processes in shock ignited gases by the use of laser shear interferometry, Combust. Sci. Tech. 8 (1973) 185-197.

4.   L. Bates, D. Bradley, G. Paczko, N. Peters, Engine hot spots: Modes of auto-ignition and reaction propagation, Combust. Flame 166 (2016) 80-85.

5.   D. Bradley, G. Kalghatgi, Influence of autoignition delay time characteristics of different fuels on pressure waves and knock in reciprocating engines, Combust. Flame 156 (2009) 2307-2318.

6.   G. P. Smith, D. M. Golden, M. Frenklach, N. W. Moriarty, B. Eiteneer, M. Goldenberg, C. T. Bowman, R. K. Hanson, S. Song, W. C. Gardiner Jr, GRI-Mech 3.0, (1999). Available: http://www. me. berkeley. edu/gri_mech (accessed 15/05/2016).

7.   U. Burke, K. P. Somers, P. O'Toole, C. M. Zinner, N. Marquet, G. Bourque, E. L. Petersen, W. K. Metcalfe, Z. Serinyel, H. J. Curran, An ignition delay and kinetic modeling study of methane, dimethyl ether, and their mixtures at high pressures, Combust. Flame 162 (2015) 315-330.

8.   D. Goodwin, Cantera: Object-oriented software for reacting flows, (2005). Available: http://www. cantera. org (accessed 17/10/2016).

9.   Design Reaction, CHEMKIN 10131, React. Des. (2013).

10.   S. Gordon, B. J. McBride, Computer program for calculation of complex chemical equilibrium compositions and applications, Citeseer, 1996.

11.   M. Schreiber, A. S. Sakak, A. Lingens, J. Griffiths, A reduced thermokinetic model for the autoignition of fuels with variable octane ratings, Symp. (Int.) Combust. 25 (1994) 933-940.

12.   W. K. Metcalfe, S. M. Burke, S. S. Ahmed, H. J. Curran, A hierarchical and comparative kinetic modeling study of C1− C2 hydrocarbon and oxygenated fuels, Int. J. Chem. Kinet. 45 (2013) 638-675.

13.   J. Huang, P. G. Hill, W. K. Bushe, S. R. Munshi, Shock-tube study of methane ignition under engine-relevant conditions: experiments and modeling, Combust. Flame 136 (2004) 25-42.

14.   U. Müller, N. Peters, A. Linan, Global kinetics for n-heptane ignition at high pressures, Symp. (Int.) Combust. 24 (1992) 777-784.

15.   E. Hu, X. Li, X. Meng, Y. Chen, Y. Cheng, Y. Xie, Z. Huang, Laminar flame speeds and ignition delay times of methane–air mixtures at elevated temperatures and pressures, Fuel 158 (2015) 1-10.

16.   J. Herzler, C. Naumann, Shock-tube study of the ignition of methane/ethane/hydrogen mixtures with hydrogen contents from 0% to 100% at different pressures, Proc. Combust. Inst. 32 (2009) 213-220.

17.   C. Trevino, F. Mendez, Reduced kinetic mechanism for methane ignition, Symp. (Int.) Combust. 24 (1992) 121-127.

18.   W. Zeng, H. Ma, Y. Liang, E. Hu, Experimental and modeling study on effects of N_2 and CO_2 on ignition characteristics of methane/air mixture, J. Adv. Res. 6 (2015) 189-201.

19.   J. Huang, W. Bushe, Experimental and kinetic study of autoignition in methane/ethane/air and methane/propane/air mixtures under engine-relevant conditions, Combust. Flame 144 (2006) 74-88.

20.   S.-K. Kim, Y. Yu, J. Ahn, Y.-M. Kim, Numerical investigation of the autoignition of turbulent gaseous jets in a high-pressure environment using the multiple-RIF model, Fuel 83 (2004) 375-386.

21.   J. Huang, P. Hill, W. Bushe, S. Munshi, Shock-tube study of methane ignition under engine-relevant conditions: experiments and modeling, Combust. Flame 136 (2004) 25-42.

22.   H. El Merhubi, A. Kéromnès, G. Catalano, B. Lefort, L. Le Moyne, A high pressure experimental and numerical study of methane ignition, Fuel 177 (2016) 164-172.

23.   M. Frenklach, H. Wang, M. J. Rabinowitz, Optimization and analysis of large chemical kinetic mechanisms using the solution mapping method—combustion of methane, Progress Energy Combust. Sci. 18 (1992) 47-73.

24.   C. J. Aul, W. K. Metcalfe, S. M. Burke, H. J. Curran, E. L. Petersen, Ignition and kinetic modeling of methane and ethane fuel blends with oxygen: A design of experiments approach, Combust. Flame 160 (2013) 1153-1167.

25.   T. Nagy, É. Valkó, I. Sedyó, I. G. Zsély, M. J. Pilling, T. Turányi, Uncertainty of the rate parameters of several important elementary reactions of the H_2 and syngas combustion systems, Combust. Flame 162 (2015) 2059-2076.

26.   T. Varga, C. Olm, T. Nagy, I. G. Zsély, É. Valkó, R. Pálvölgyi, H. Curran, T. Turányi, Development of a joint hydrogen and syngas combustion mechanism based on an optimization approach, Int. J. Chem. Kinet. (2016).

27.   M. P. Burke, S. J. Klippenstein, L. B. Harding, A quantitative explanation for the apparent anomalous temperature dependence of $OH+ HO_2= H_2O+ O_2$ through multi-scale modeling, Proc. Combust. Inst. 34 (2013) 547-555.

28.   D. Bradley, How fast can we burn?, Symp. (Int.) Combust. 24 (1992) 247-262.

29.   D. Bradley, Autoignitions and detonations in engines and ducts, Philos. Trans. R. Soc. London, Ser. A 370 (2012) 689-714.

30.   M. Radulescu, G. Sharpe, D. Bradley, A Universal Parameter Quantifying Explosion Hazards, Detonability and Hot Spot Formation: The χ Number, Proc. 7th Int. Semin. Fire Explos. Hazards (D. Bradley, G. Makhviladze, V. Molkov, P. Sunderland, and F. Tamanini, Eds.) (2013) 617-626.

31.   D. Bradley, R. A. Head, Engine autoignition: the relationship between octane numbers and autoignition delay times, Combust. Flame 147 (2006) 171-184.

32.   L. Bates, D. Bradley, Deflagrative, auto-ignitive, and detonative propagation regimes in engines, Combust. Flame 175 (2017) 118-122.

33.   Jiaying Pan, Haiqiao Wei, Gequn Shu, Zheng Chen, Peng Zhao, The role of low temperature chemistry in combustion mode development under elevated pressures, Combust. Flame 174 (2016) 179-193.

34.   R. Sankaran, H. G. Im, E. R. Hawkes, J. H. Chen, The effects of non-uniform temperature distribution on the ignition of a lean homogeneous hydrogen–air mixture, Proc. Combust. Inst. 30 (2005) 875-882.

35.   C. Strozzi, A. Mura, J. Sotton, M. Bellenoue, Experimental analysis of propagation regimes during the autoignition of a fully premixed methane–air mixture in the presence of temperature inhomogeneities, Combust. Flame 159 (2012) 3323-3341.

36.   A. B. Mansfield, M. S. Wooldridge, High-pressure low-temperature ignition behavior of syngas mixtures, Combust. Flame 161 (2014) 2242-2251.

37.   A. B. Mansfield, M. S. Wooldridge, H. Di, X. He, Low-temperature ignition behavior of iso-octane, Fuel 139 (2015) 79-86.

38.   G. Kalghatgi, I. Algunaibet, K. Morganti, On knock intensity and superknock in SI engine, SAE 2017-01-0689 (2017).

39.   D. Bradley, C. Morley, X. Gu, D. Emerson, Amplified pressure waves during autoignition: relevance to CAI engines, SAE paper 2002-01-2868,   (2002).